LUPINE PUBLISHERS

Scholarly Journal of Food and Nutrition

DOI: 10.32474/SJFN.2021.03.000171

ISSN: 2638-6070

Research Article

Assessment of Physicochemical, Spectroscopic, and Thermal Properties of Energy of Consciousness Treated Sodium Selenate

Mahendra Kumar Trivedi[1] and Snehasis Jana[2]*

[1]*Trivedi Global, Inc., Henderson, USA*

[2]*Trivedi Science Research Laboratory Pvt. Ltd., Thane (West), Maharashtra, India*

***Corresponding author:** Snehasis Jana, Trivedi Science Research Laboratory Pvt. Ltd., Thane (West), Maharashtra, India.

Received: January 19, 2021 **Published:** January 29, 2021

Abstract

Selenium is one of the important nutrients that are essential in the body for a healthy metabolism. Sodium selenate is the inorganic form of selenium used in several supplements for the prevention and treatment of different disorders. The objective of this study was to determine the impact of The Trivedi Effect®-The Energy of Consciousness Healing Treatment on the physicochemical, spectroscopic, and thermal properties of sodium selenate. In this regard, sodium selenate was divided in two parts among which one part was kept untreated and termed as control sample. Besides, the another part was treated remotely with The Trivedi Effect®-Biofield Energy Healing Treatment by the renowned Biofield Energy Healer, Mr. Mahendra Kumar Trivedi and referred as Biofield Energy Treated sample. Consequently, both the samples were analysed using various analytical techniques such as PXRD, PSA, FT-IR, UV-Vis, TGA, and DSC. The PXRD analysis of the treated sample showed the significant changes from -11.10% to +50% in the crystallite sizes along with 4.2% increase in average crystallite size as compared to the control sample. Besides, the particle sizes d_{10}, d_{50}, d_{90}, and D (4,3) values of the treated sample were found to be significantly reduced by 51.61%, 38.79%, 25.31%, and 33.05%, respectively as compared to the control sample. Moreover, the treated sample also showed 70.99% increase in surface area as compared to the control sample. The TGA analysis of the treated sample revealed 60.96% increased weight loss than the control and the maximum degradation temperature (T_{max}) was also reported to be decreased by 21.67% as compared to control. The DSC studies showed the slight lowering (0.95%) in the melting point of treated sample along with 31.37% significant increase in the latent heat of fusion compared with the control sample. However, the FT-IR and UV-Vis of Biofield Energy Treated sample did not reveal any significant alteration, as compared with the spectra of the control sample. The overall analysis revealed that The Trivedi Effect®- Energy of Consciousness Healing Treatment might alter the crystal morphology of sodium selenate. Moreover, the treated sample showed reduced particle size along with increased surface area that may enhance the solubility, absorption and bioavailability parameters of sodium selenate. Thus, the Trivedi Effect® Treated sodium selenate would be useful for designing the better nutraceutical and/or pharmaceutical preparations that could offer better therapeutic response against inflammatory diseases, immunological disorders, stress, aging, heart diseases, infectious diseases, diabetes, cancer, Alzheimer's disease, etc.

Keywords: Sodium Selenate; Energy of Consciousness Healing Treatment; The Trivedi Effect®; PXRD; Particle Size; FTIR; DSC; TGA

Introduction

In human, the diet plays crucial role regarding the aetiology, prevention and treatment of various diseases and it is already demonstrated and established by several scientific studies [1-3]. The proper diet is known for providing various nutrients to the body and selenium (Se) is one among of those nutrients that is important in terms of the healthy metabolism of the human body. Se could be obtained from several foods that act as the natural source however, its level in food basically depends on the soil Se level. Se is well-known for its neuro-protective actions [4] and antioxidant functions [5]. Besides, the imbalanced level of Se inside body is found to be involved in the pathophysiology of several diseases, such as type-2 diabetes, cancer, cardiovascular disease, viral diseases, male infertility, muscle disorders, and neurological disorders, etc. [6-8]. Se plays an important role in selenoproteins

Copyright © All rights are reserved by Mahendra Kumar Trivedi.

that act as antioxidants and protect the body against the oxidative stress caused due to the excess reactive nitrogen species (NOS) and reactive oxygen species (ROS), and such activities attract various researchers to show their interest in Se based research works, in recent years [9-10]. Apart from that, Se is also present in biological materials in different chemical forms, i.e., either organic forms, such as selenomethionine and dimethylselenide, or inorganic selenites and selenates. Among such forms, selenomethionine is an important source of dietary Se, as Se is mainly present in this form in various food materials [11]. Moreover, the same chemical form is also used for Se supplements in various clinical trials. Clinically, the supplements containing Se are important for those populations that may not easily consume it through diet due to living in such geographical areas or may have such genetic variations that further alter its metabolism [12]. Since the low level of Se in body may create concern for associated deficiency diseases; it leads to the enactment of the recommended daily requirements in several countries. However, if its use is not properly regulated, the excess Se intakes due to the use of supplements or their misuse as health therapy may also cause adverse health effects [13].

The absorption rate of Se in selenite form is more than 80 percent. However, in selenomethionine or selenate form, it may be more than 90 percent. Therefore, sodium selenate was included as one component in the novel proprietary herbo-mineral formulation as the selenium ion source. Such herbo-mineral formulation is delineated in the form of nutraceutical supplement that has the wide uses in terms of the prevention as well as treatment of various disorders [14-15]. Since the physicochemical properties of a drug plays crucial role in its absorption and bioavailability profile as well as the stability of the drug [16], the researchers pay their attention to improve such parameters of the drug. In this scenario, it was observed that Biofield Energy Healing Treatment (The Trivedi Effect®) has the considerable impact on various properties of drug moiety such as, particle size, surface area, and other chemical and thermal behaviour, through possible mediation of neutrinos [17-19]. Every living organism possess some kind of unique energy known as Biofield Energy, which is infinite, para-dimensional and electromagnetic field surrounding the human body. Biofield (Putative Energy Fields) based Energy Healing Therapies have been reported to have significant outcomes against various disease conditions [20]. National Institute of Health/ National Center for Complementary and Alternative Medicine (NIH/NCCAM) recommend and included the Energy therapy under Complementary and Alternative Medicine (CAM) category that has been accepted by the most of the U.S. population with several advantages [21]. The Trivedi Effect®-Consciousness Energy Healing has been widely reported for altering the physicochemical properties of metals, ceramics, polymers, and organic compounds [22-24], nutraceuticals [25-26], and its impact in pharmaceutical products [27-28], livestock [29], agricultural science [30-31], and skin health [32-33]. The Energy of Consciousness has also been found to be effective in reducing the particle size with the improvement of the surface area that would be advantageous regarding the enhancement of the solubility and bioavailability of pharmaceutical/nutraceutical compounds [34-35]. Thus, this study was designed to determine the impact of the Biofield Energy Healing Treatment on the physicochemical, spectroacopic, and thermal properties of sodium selenate with the help of various analytical techniques such as, PXRD, PSA, FT-IR spectrometry, UV-vis spectroscopy, TGA/DTG, and DSC.

Materials and Methods

Chemicals and Reagents

Sodium selenate was procured from Alfa Aesar, USA. The other chemicals used in the experiment were of analytical grade available in India.

Consciousness Energy Healing Treatment Strategies

The test compound i.e., sodium selenate was divided into two parts among which, one part did not receive the Biofield Energy Treatment and therefore considered as control sodium selenate. The second part of the test compound received the Energy of Consciousness Healing Treatment by the renowned Biofield Energy Healer, Mr. Mahendra Kumar Trivedi (USA), and it was labelled as the Biofield Energy Treated sodium selenate. In this process, the Healer remotely provided the Trivedi Effect® - Energy of Consciousness Healing Treatment to the sample for 3 minutes through the Unique Energy Transmission process, which was placed under the standard laboratory conditions. On the other hand, the control sample was subjected to "sham" healer, who did not have any knowledge about the Biofield Energy Treatment, under the similar laboratory conditions. Later on, the control and Biofield Energy Treated samples were kept in similar sealed conditions and characterized using PXRD, PSA, FTIR, UV-Vis, TGA/DTG, and DSC techniques.

Characterization

Powder X-ray Diffraction (PXRD) Analysis

The PXRD analysis of sodium selenate was done using PANalytical X'Pert3 powder X-ray diffractometer, UK. The copper line was used as the source of radiation for diffraction of the analyte at 0.154 nm X-ray wavelength that is running at 40 mA current and 45 kV voltage. Moreover, the instrument uses a scanning rate of 18.87°/second over a 2θ range of 3-90° and the ratio of Kα-2 and Kα-1 was 0.5 (k, equipment constant). The data was collected using X'Pert data collector and X'Pert high score plus processing software in the form of a chart of the Bragg angle (2θ) *vs.* intensity (counts per second), and a detailed table containing information on peak intensity counts, d value (Å), full width half maximum (FWHM) (°2θ), relative intensity (%), and area (cts*°2θ). The crystallite size (G) was calculated by using the Scherrer equation (1) as follows:

$$G = k\lambda/(b\cos\theta) \quad (1)$$

Where, k is the equipment constant (0.5), λ is the X-ray wavelength (0.154 nm); b in radians is the full width at half of the peaks and θ is the corresponding Bragg angle.

Percent change in crystallite size (G) of sodium selenate was calculated using following equation 2:

$$\%\ \text{change in crystallite size} = \frac{[G_{\text{Treated}} - G_{\text{control}}]}{G_{\text{control}}} \times 100 \quad (2)$$

Where, $G_{Control}$ and $G_{Treated}$ are the crystallite size of the control and Biofield Energy Treated sodium selenate samples, respectively.

Particle Size Analysis (PSA)

The particle size analysis of the samples were done using wet method, which is conducted on Malvern Mastersizer 3000, UK with a detection range between 0.01 µm to 3000 µm [34]. In this method, the sample unit (Hydro MV) was filled with light liquid paraffin oil (act as dispersant medium) and stirred at 2500 rpm. The refractive index values for dispersant medium and samples were 0.0 and 1.47, respectively. The measurement was taken twice after reaching obscuration in between 10% and 20%, followed by averaging the two measurements. The PS analysis provides data in the form of d_{10} µm, d_{50} µm, and d_{90} µm, representing the particle diameter corresponding to 10%, 50%, and 90% of the cumulative distribution. D (4, 3) µm represents the average mass-volume diameter and SSA is the specific surface area (m^2/Kg). The calculations were done by using software Mastersizer V3.50.

The percent change in particle size (d) for d_{10}, d_{50}, d_{90} and D (4,3) was calculated using following equation 3:

$$\%\ \text{change in particle size} = \frac{[d_{\text{Treated}} - d_{\text{Control}}]}{d_{\text{Control}}} \times 100 \quad (3)$$

Where, $d_{Control}$ and $d_{Treated}$ are the particle size (µm) for at below 10% level (d_{10}), 50% level (d_{50}), and 90% level (d_{90}) of the control and Biofield Energy Treated samples, respectively.

Percent change in surface area (S) was calculated using following equation 4:

$$\%\ \text{change in specific surface area} = \frac{[S_{\text{Treated}} - S_{\text{Control}}]}{S_{\text{Control}}} \times 100 \quad (4)$$

Where, $S_{Control}$ and $S_{Treated}$ are the surface area of the control and Biofield Energy treated sodium selenate, respectively.

Fourier Transform Infrared (FT-IR) Spectroscopy

FT-IR spectroscopy of sodium selenate was performed on Spectrum ES Fourier transform infrared spectrometer (Perkin Elmer, USA) by using pressed KBr disk technique with the frequency array of 400-4000 cm^{-1}. The technique uses ~2 mg of control sample and about 300 mg of KBr as the diluent to form the pressed disk followed by running the sample in the spectrometer. The same procedure was adopted for the Biofield Energy Treated sample.

Ultraviolet-visible Spectroscopy (UV-Vis) Analysis

The UV-Vis spectral analysis of the control and treated sodium selenate samples were carried out using Shimadzu UV-2400 PC SERIES with UV Probe (Shimadzu, JAPAN). The spectrum was recorded in the wavelength range of 190-800 nm using 1 cm quartz cell that has a slit width of 0.5 nm. The absorbance spectra (in the range of 0.2 to 0.9) and wavelength of maximum absorbance (λ_{max}) were recorded.

Thermal Gravimetric Analysis (TGA) / Differential thermogravimetric analysis (DTG)

TGA/DTG thermograms of control and treated sodium selenate samples were obtained in a TGA Q500 themoanalyzer apparatus, USA under dynamic nitrogen atmosphere (50 mL/min). It involves the use of platinum crucible and the heating rate of 10 ºC/min from 25 °C to 800 °C [35]. In TGA analysis, the weight loss in gram as well as percent loss for each step was recorded with respect to the initial weight of the sample. In DTG analysis, the onset, endset, peak temperature and integral area for each peak was recorded. The percent change in weight loss (W) was calculated using following equation 5:

$$\%\ \text{change in weight loss} = \frac{[W_{\text{Treated}} - W_{\text{control}}]}{W_{\text{control}}} \times 100 \quad (5)$$

Where, $W_{Control}$ and $W_{Treated}$ are the weight loss of the control and Biofield Energy Treated samples, respectively.

Also, the percent change in maximum thermal degradation temperature (T_{max}) (M) was calculated using following equation 6:

$$\%\ \text{change in } T_{max}\ (M) = \frac{[M_{\text{Treated}} - M_{\text{Control}}]}{M_{\text{Control}}} \times 100 \quad (6)$$

Where, $M_{Control}$ and $M_{Treated}$ are the T_{max} values of the control and Biofield Energy Treated samples, respectively.

Differential Scanning Calorimetry (DSC)

The DSC analysis of the samples was performed using DSC Q2000 differential scanning calorimeter, USA under the dynamic nitrogen atmosphere with flow rate of 50 mL/min. It includes a sample mass of ~2.5 mg using aluminum pan which is heated at the rate of 10 ºC/min from 30 °C to 450 °C [35]. Later on, the percent change in melting point (T) of the control and treated samples was calculated using following equation 7:

$$\%\ \text{change in melting point} = \frac{[T_{\text{Treated}} - T_{\text{Control}}]}{T_{\text{Control}}} \times 100 \quad (7)$$

Where, $T_{Control}$ and $T_{Treated}$ are the melting point of the control and treated sodium selenate samples, respectively.

Also, the percent change in the latent heat of fusion (ΔH) was calculated using following equation 8:

$$\%\ \text{change in latent heat of fusion} = \frac{[\Delta H_{\text{Treated}} - \Delta H_{\text{Control}}]}{\Delta H_{\text{Control}}} \times 100 \quad (8)$$

Where, $\Delta H_{Control}$ and $\Delta H_{Treated}$ are the latent heat of fusion of the control and treated sodium selenate, respectively.

Result and Discussion

Powder X-ray Diffraction (PXRD) Analysis

The PXRD diffractograms of both the control and treated sodium selenate samples (Figure 1) showed very sharp and intense peaks with no broadening peaks, which shows that both samples were crystalline in nature. The PXRD data for the control and treated sodium selenate samples, including Bragg angle (2θ), relative intensity (%), and crystallite size (G) are presented in Table 1. The crystallite size was calculated with the use of Scherrer equation [36]. The PXRD diffractograms of both samples showed the highest peak intensity (100%) at Bragg's angle (2θ) equal to 18.4° (Table 1, entry 1); however, significant alterations were found in the relative intensities of other XRD peaks in the Biofield Energy Treated sample as compared to the control sample. The overall peak intensities of the Biofield Energy Treated sample was altered in the range from -46.68% to +17.02%. The analysis revealed that the crystallite sizes of the Biofield Energy Treated sample were significantly decreased in the range of 11.10% to 31.27% at 2θ equal to nearly 45.1°, 56.2°, 68.3°, and 70.2° (Table 1, entry 9, 14, 21, and 22) with respect to the control sample. Furthermore, the crystallite sizes at position 2θ equal to nearly 18.4°, 28.4°, 37.2°, 45.9°, 57.4°, 59.1°, 60.2°, 65.0°, and 65.3° (Table 1, entry 1, 4, 8, 10, 15, 16, 17, 19, and 20) of the Biofield Energy Treated samples were significantly increased in the range of 8.33% to 50.0% as compared to the control sample. Also, the average crystallite size of the Biofield Energy Treated sample was found increased by 4.2% as compared to the control sample. Some studies reported that the change in the crystal morphology may cause the alterations in the relative intensities of the peaks [37]. Thus, it is assumed that the Biofield Energy Treatment might transfer some energy in the sample, which probably altered the polymorphic form or crystal morphology of sodium selenate molecules. Polymorphic forms of drugs are responsible for alterations in the performance of drugs, such as efficacy, bioavailability, and toxicity profiles, due to alteration in their physicochemical and thermodynamic properties from the original form. Also, it is well known that the absorption and bioavailability parameters of any drug are highly impacted due to the crystallite size and polymorphic form of that drug [38], thus the Energy of Consciousness Healing Treatment might be considered as a useful approach regarding the bioavailability enhancement of sodium selenate.

Table 1: PXRD data for the control and Biofield Energy Treated sodium selenate.

Entry No.	Bragg angle (°2q)	Relative Intensity (%)			Crystallite size (G, nm)		
		Control	Treated	% change [a]	Control	Treated	% change [b]
1	18.4	100	100	0	38.83	43.69	12.51
2	22.5	29.3	27.03	-7.74	35.17	35.17	0
3	27.3	58.76	47.47	-19.21	50.72	50.72	0
4	28.4	28.25	27.17	-3.82	41.67	50.85	22.01
5	31	65	60.47	-6.97	36.69	36.69	0
6	32.6	63.17	50.77	-19.63	49.11	49.11	-0.01
7	34.3	4.16	3.15	-24.28	42.28	42.28	0
8	37.2	15.14	13.07	-13.67	22.96	24.87	8.33
9	45.1	5.43	3.8	-30.02	51.03	43.74	-14.29
10	45.9	3.82	4.47	17.02	38.39	43.87	14.29
11	47.4	20.41	15.78	-22.68	44.12	44.12	0
12	48.8	10.59	7.81	-26.25	44.37	44.37	0
13	53	21.78	13.63	-37.42	45.14	45.14	0
14	56.2	2.71	1.83	-32.47	40.07	35.63	-11.1
15	57.4	4.43	3.45	-22.12	35.82	53.73	50
16	59.1	3.73	2.64	-29.22	40.64	46.44	14.27
17	60.2	5.46	3.57	-34.61	40.86	46.69	14.28
18	62.7	3.28	2.97	-9.45	36.79	36.79	0
19	65	2.18	2.39	9.63	33.54	41.92	25
20	65.3	4.92	3.42	-30.49	33.58	37.31	11.1
21	68.3	5.02	3.67	-26.89	42.72	37.97	-11.12
22	70.2	4.97	2.65	-46.68	31.43	21.6	-31.27

[a]denotes the percentage change in the relative intensity of Biofield Energy Treated sample with respect to the control sample; [b]denotes the percentage change in the crystallite size of Biofield Energy Treated sample with respect to the control sample

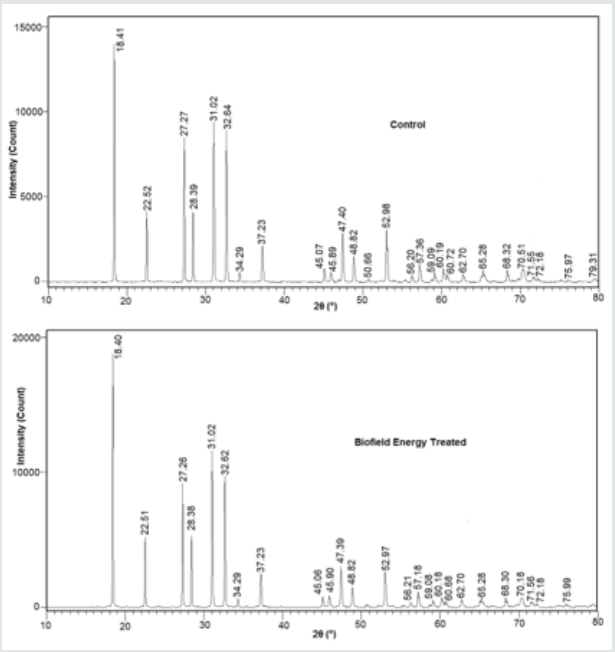

Figure 1: XRD diffractograms of the control and Biofield Energy Treated sodium selenate.

Particle Size Distribution (PSD) Analysis

Particle sizes ($d_{10,}$ $d_{50,}$ and d_{90}) as well as the surface area of both the control and treated sodium selenate samples were analysed and the results are presented in Table 2. The size of the particles at below 10% level (d_{10}), 50% level (d_{50}), and 90% level (d_{90}) of the treated sodium selenate were significantly reduced by 51.61%, 38.79%, and 25.31%, respectively as compared to the control sample. Similarly, the average mass-volume diameter, D(4,3) of the treated sample was also reduced by 33.05% as compared to the control sodium selenate. Apart from that, the surface area analysis (Table 2) showed a significant increase in surface area of the Biofield Energy Treated sample (70.99%) as compared to the control sample. The reason behind decreased particle size may be that the Biofield Energy Treatment might fracture the internal boundaries of particles and that resulted into the particles of smaller size [39]. Later on, the increased surface area of treated sample might be due to this decrease in particle size of sodium selenate as compared to the control sample. Moreover, particle size and surface area are considered as the important parameters that play their role in the dissolution of the drug. Hence, it could be considered that the Biofield Energy Treatment might be suitable for increasing the solubility and rate of dissolution as well as absorption of sodium selenate.

Table 2: Particle size distribution of the control and Biofield Energy Treated sodium selenate.

Test Item	d_{10} (µm)	d_{50} (µm)	d_{90} (µm)	D(4,3) (µm)	SSA(m^2/Kg)
Control sample	24.8	64.2	128	70.8	146.5
Biofield Energy Treated sample	12	39.3	95.6	47.4	250.5
Percent change* (%)	-51.61	-38.79	-25.31	-33.05	70.99

d_{10}, d_{50}, and d_{90}: particle diameter corresponding to 10%, 50%, and 90% of the cumulative distribution, D(4,3) : the average mass-volume diameter, and SSA : the specific surface area; *denotes the percentage change in the Particle size distribution of the Biofield Energy Treated sample with respect to the control sample.

Fourier Transform Infrared (FT-IR) Spectroscopy

The FT-IR spectra of both the control as well as treated sodium selenate samples are presented in Figure 2. The spectra of control and treated sample showed a broad peak at 3448 and 3444 cm^{-1}, respectively that represents the O-H stretching vibration. Similarly, the peak at 1720 cm^{-1} in both samples is may be due to the O-H bending vibrations. These vibrations might be shown in the spectra due to the presence of water molecules in the samples that may get incorporated into the lattice structure of the crystalline inorganic compound. Moreover, the literature reported the metal oxide stretching peak in the range of 1010-850 cm^{-1} [40]. In these spectra, the sharp and strong peak at 884 cm^{-1} in both the control and treated sample is due to the Se-O stretching in the fingerprint region. The analysis revealed that the fingerprint region of both the samples remained same and the FT-IR spectra did not revealed any significant changes in the vibrational frequencies between the control and treated samples. Thus, it may be concluded that Biofield Energy Treatment might not produce any alteration in the compound at bonding level.

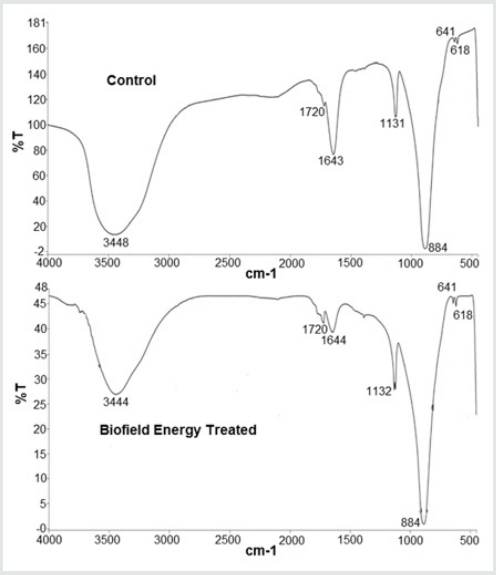

Figure 2: FT-IR spectra of the control and Biofield Energy Treated sodium selenate.

Ultraviolet-visible Spectroscopy (UV-Vis) Analysis

The UV-visible spectra of both the control and treated sodium selenate samples are shown in Figure 3.

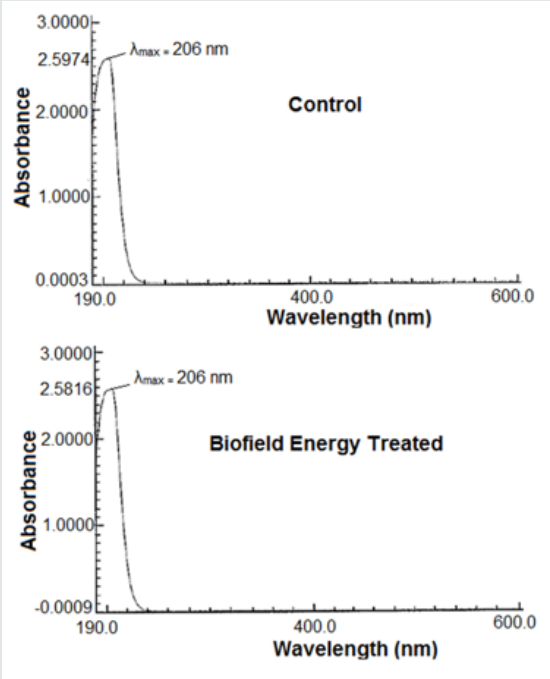

Figure 3: UV-vis spectra of the control and Biofield Energy Treated sodium selenate.

The UV spectra of both, control and Biofield Energy Treated samples, showed the maximum absorbance (λ_{max}) at 206 nm. Also, there is no significant alteration in the absorbance maxima between control (2.5974) and Biofield Energy Treated sample (2.5816), which shows that the Biofield Energy Treatment might not induces any significant change in the electronic transitions between highest occupied molecular orbital and lowest unoccupied molecular orbital.

Thermal Gravimetric Analysis (TGA) / Differential thermogravimetric analysis (DTG)

TGA analysis may help in revealing the information regarding the physical phenomena occurring in the compound, such as sublimation, vaporization, absorption and desorption. The thermogram also helps in possible interpretation about thermal stability, oxidation, and combustion of the compound on the basis of which, its handling, processing, storage, and shipment temperature could be decided [41]. Hence, the thermal profile and stability of control and treated sodium selenate samples were analysed using TGA and DTG analysis.

The TGA thermograms of both the control and treated samples are shown in Figure 4 and their data are presented in Table 3. The analysis revealed four steps of thermal degradation of both, control and treated sodium selenate samples. The result showed significant increase in percentage weight loss in the Biofield Energy Treated sample by 220% and 112% in the 1st and 2nd steps of degradation (Table 3) as compared to the control sample. Moreover, the overall weight loss was significantly increased by 60.96% in the Biofield Energy Treated sample as compared with the control sample. On the other hand, the DTG thermogram shows maximum thermal degradation temperature (T_{peak}) of the control sample at 87.64°C; whereas for Biofield Energy Treated sample,T_{peak} was observed at 68.65°C (Table 4). Moreover, the onset degradation temperature for control sample was observed at 79.33°C, but it was shifted to 60.39°C for the Biofield Energy Treated sample. Similarly, the end-set degradation temperature was also decreased in the treated sample (102.27°C) as compared to the control (104.27°C). Overall, TGA/DTG studies showed that the thermal stability of the Biofield Energy Treated sample was significantly reduced as compared to the control sample. The analysis also revealed the decrease in decomposition temperature of the treated sample with respect to the control sample. The previous studies reported that thermal stability of compound is directly related with the particle size [42]. Hence, it may be assumed that the resultant decrease in thermal stability of the treated sample might occurr due to the decrease in the particle size of the treated sample as compared to the control. Also, the reduced thermodynamic stability favors the increase in dissolution rate and bioavailability of the pharmaceutical compound [43], thus the treated sample may show the improved dissolution and bioavailability profile as compared to the control sample.

Table 3: Thermal degradation steps of the control and Biofield Energy Treated sodium selenate.

Step	Temperature (°C)		Weight loss %		% Change*
	Control	Treated	Control	Treated	
1st step of degradation	199.93	200.64	0.3	0.96	220
2nd step of degradation	795.64	795.25	2.62	3.74	112
Total weight loss	-	-	2.92	4.7	60.96
*denotes the percentage change in the weight loss of Biofield Energy Treated sample with respect to the control sample.					

Table 4: The maximum thermal degradation (Tmax) of the control and Biofield Energy Treated samples of sodium selenate.

Description	T_{onset} (°C)	T_{peak} (°C)	T_{endset} (°C)
Control Sample	79.33	87.64	104.27

Treated Sample	60.39	68.65	102.27
%Change*	-23.87	-21.67	-1.92

T_{onset}: Onset temperature, T_{peak}: Peak temperature, T_{endset}: Endset temperature, *denotes the percentage change of the Biofield Energy Treated sample with respect to the control sample.

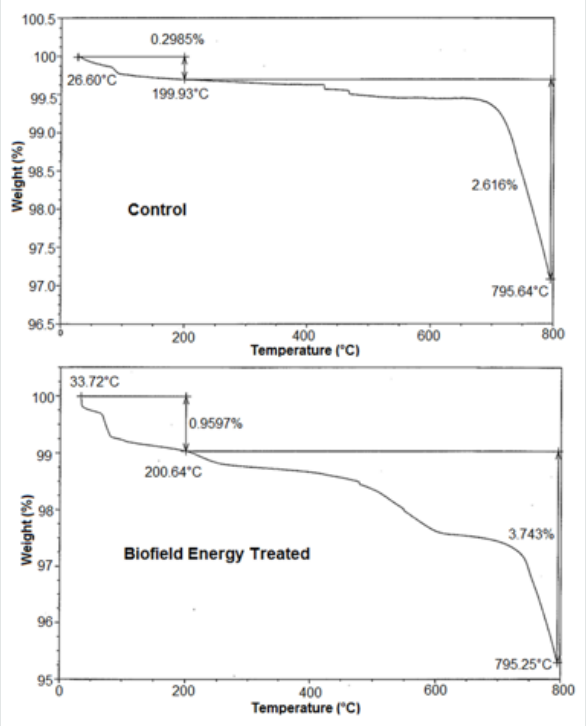

Figure 4: TGA thermograms of the control and Biofield Energy Treated sodium selenate.

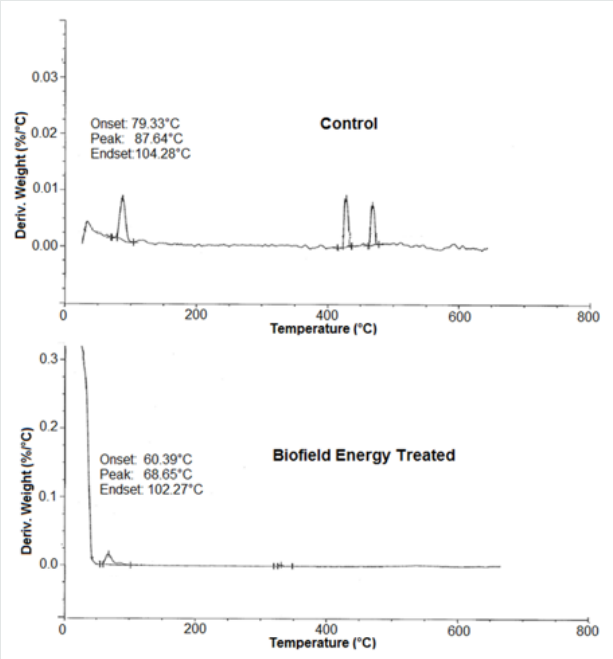

Figure 5: DTG thermograms of the control and Biofield Energy Treated sodium selenate.

Differential Scanning Calorimetry (DSC) Analysis

The DSC analysis was used for determining the melting point and latent heat of fusion (ΔH) of both, the control and Biofield Energy Treated samples. The DSC thermograms of control and treated sodium selenate are shown in Figure 6 and results are presented in Table 5. The onset vaporisation temperature for control sample was observed at 86.53°C, whereas, in treated sample, it was found at 87.43°C that shows a slight increase (1.04%) as compared to the control. However, the endset temperature of treated sample was observed at 111.99°C, which represent -3.94% reductions as compared to the control (116.58°C). The data also showed a slight lowering of the vaporisation temperature (0.95%) in the Biofield Energy Treated sodium selenate (91.75°C) as compared to the control sample (92.63 °C). Besides, the latent heat of vaporisation of Biofield Energy Treated sample was found to be significantly increased by 31.37% as compared to the control. Several studies reported that the vaporisation temperature of compound is related to its kinetic energy [44]. Hence, based on this, it may be assumed that the Biofield Energy Treatment might enhance the internal energy of treated sample, which led to increase in the latent heat of vaporisation and consequently decrease in the vaporisation temperature as compared to the control sample.

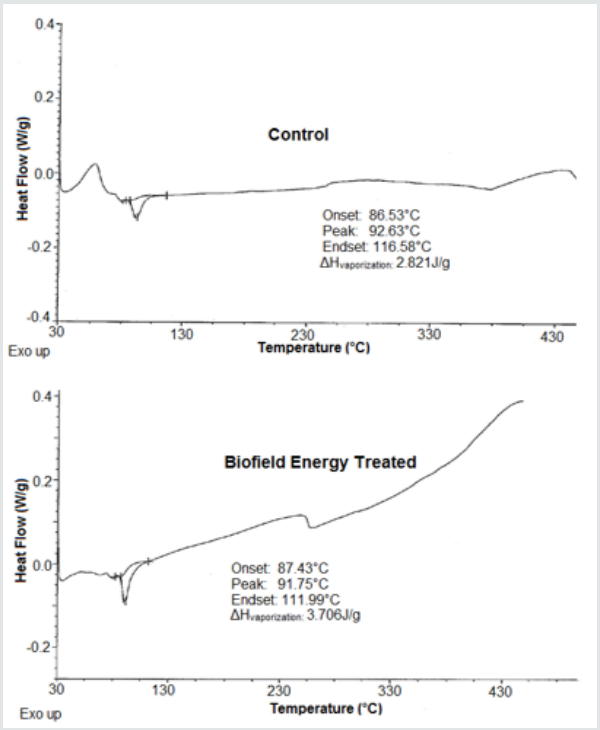

Figure 6: DSC thermograms of the control and Biofield Energy Treated sodium selenate.

Table 5: Comparison of DSC data between the control and Biofield Energy Treated sodium selenate.

Entry No.	Sample	$\Delta H_{vaporisation}$ (J/g)	T_{onset} (°C)	T_{peak} (°C)	T_{endset} (°C)
1	Control	2.821	86.53	92.63	116.58
2	Trivedi Effect® Treated	3.706	87.43	91.75	111.99
3	% Change*	31.37	1.04	-0.95	-3.94

T_{onset}: Onset vaporisation temperature, T_{peak}: Peak vaporisation temperature, T_{endset}: Endset vaporisation temperature, ΔHfusion: Latent heat of vaporisation, *denotes the percentage change of Biofield Energy Treated sample with respect to the control sample.

Conclusion

The study concluded the significant impact of The Trivedi Effect®- Energy of Consciousness Healing Treatment on the physicochemical as well as thermal properties of sodium selenate. The PXRD analysis showed alteration in the relative peak intensities along with the crystallite size of the treated sample as compared to the control. The crystallize size of treated sample shows changes in the range of -11.10% to 50.0% with 4.2% increase in the average crystallite size. It designates the impact of Biofield Energy treatment on the crystal morphology of the treated sodium selenate sample. The particle sizes of treated sodium selenate sample was also found reduced as the values of d_{10}, d_{50}, $d_{90,}$ and D (4,3) were reduced by 51.61%, 38.79%, 25.31%, and 33.05%, respectively in comparison to the values of control sample. The surface area analysis of the control and treated sample also revealed a remarkable change in the treated sample that was increased by 70.99% when compared with the control sample. Such changes in the particle size and surface area of treated sodium selenate may be occurred, because the Biofield Energy Treatment might act on the internal boundaries of particles and fracture them to create the smaller sized particles. Additionally, the thermal analysis done by TGA/DTG revealed the increase in total weight loss of the treated sample by 60.96% and reduction in T_{peak} by 21.67% as compared with the control sample. It shows the decrease in the thermal stability of the Biofield Energy Treated sample which might be due to decrease in the particle size of the treated sample. The DSC analysis showed that vaporisation temperature of the treated sample was slightly reduced, while ΔH revealed 31.37% increase than the control sample. The reason behind this alteration may be due to increase in the internal energy of treated sample through the Biofield Energy Treatment. However, the spectral analysis did not reveal any significant changes between the control and treated samples.

Overall, the present study showed the significant impact of Mr. Trivedi's Biofield Energy Treatment on the physicochemical and thermal properties of sodium selenate with respect to the control sample. The treated sample might possess new crystal morphology having reduced particle size and thermodynamic stability with increased surface area. Based on this, it is expected that The Trivedi Effect® may be used to enhance various properties of drugs in terms of solubility, dissolution, absorption, and bioavailability and thereby helps in designing of better nutraceutical and/or pharmaceutical formulations with more effective pharmacological actions against various diseases such as impotency, mood swings, migraines, diabetes mellitus, obsessive/compulsive behavior and panic attacks, stress-related disorders, lack of motivation, inflammatory diseases and immunological disorders, chronic infections and much more.

Acknowledgement

The authors are grateful to GVK Biosciences Pvt. Ltd., Trivedi Science, Trivedi Global, Inc., Trivedi Testimonials, and Trivedi Master Wellness for their assistance and support during this work.

Reference

1. Barnard ND, Bush AI, Ceccarelli A, Cooper J, de Jager CA, et al. (2014) Dietary and lifestyle guidelines for the prevention of Alzheimer's disease. Neurobiol Aging 35: S74-S78.
2. Chiva Blanch G, Badimon L, Estruch R (2014) Latest evidence of the effects of the Mediterranean diet in prevention of cardiovascular disease. Curr Atheroscler Rep 169(10): 1-7.
3. Squitti R, Siotto M, Polimanti R (2014) Low-copper diet as a preventive strategy for Alzheimer's disease. Neurobiol Aging 35: S40-S50.
4. Yang X, Bao Y, Fu H, Li L, Ren T, et al. (2014) Selenium protects neonates against neurotoxicity from prenatal exposure to manganese. PloS one 9: e86611.
5. Li X, Yin D, Yin J, Chen Q, Wang R (2014) Dietary selenium protect against redox-mediated immune suppression induced by methylmercury exposure. Food Chem Toxicol 72: 169-177.
6. Rayman MP (2012) Selenium and human health. The Lancet 379(9822): 1256-1268.
7. Hatfield DL, Tsuji PA, Carlson BA, Gladyshev VN (2014) Selenium and selenocysteine: roles in cancer, health, and development. Trends Biochem Sci 39(3): 112-120.
8. Roman M, Jitaru P, Barbante C (2014) Selenium biochemistry and its role for human health. Metallomics 6(1): 25-54.
9. Pitts MW, Byrns CN, Ogawa Wong AN, Kremer P, Berry MJ (2014) *Selenoproteins* in nervous system development and function. Biol Trace Elem Res 161(3): 231-245.
10. Tapiero H, Townsend DM, Tew KD (2003) The antioxidant role of selenium and seleno-compounds. Biomed Pharmacother 57: 134-144.
11. Tinggi U (2008) Selenium: its role as antioxidant in human health. Environ Health Prev Med 13(2): 102-108.
12. Brenneisen P, Steinbrenner H, Sies H (2005) Selenium, oxidative stress, health aspects. Mol Aspects Med 26: 256-267.
13. Levander OA, Burk RF (2006) Update of human dietary standards for selenium. In: Hatfield DL, Berry MJ, Gladyshev VN, (Eds) Selenium - its molecular biology and role in human health, Springer, New York.

14. Brinkman M, Reulen RC, Kellen E, Buntinx F, Zeegers MP (2006) Are men with low selenium levels at increased risk of prostate cancer? Eur J Cancer 42: 2463-2471.

15. Patterson BH, Zech LA, Swanson CA, Levander OA (1993) Kinetic modelling of selenium in Humans using stable isotope tracers. J Trace Elem Electrolytes Health Dis 7: 117-120.

16. Chereson R (2009) Bioavailability, bioequivalence, and drug selection. In: Makoid CM, Vuchetich PJ, Banakar UV (Eds) Basic pharmacokinetics (1st Edn) Pharmaceutical Press, London.

17. Trivedi MK, Mohan TRR (2016) Biofield energy signals, energy transmission and neutrinos. American Journal of Modern Physics 5: 172-176.

18. Hammerschlag R, Levin M, McCraty R, Bat N, Ives JA, et al. (2015) Biofield Physiology: A Framework for an Emerging Discipline. Glob Adv Health Med 4: 35-41.

19. Warber SL, Cornelio D, Straughn, J, Kile G (2004) Biofield energy healing from the inside. J Altern Complement Med 10: 1107-1113.

20. Rubik B, Muehsam D, Hammerschlag R, Jain S (2015) Biofield science and healing: history, terminology, and concepts. Glob Adv Health Med 4: 8-14.

21. Barnes PM, Bloom B, Nahin RL (2008) Complementary and alternative medicine use among adults and children: United States, 2007. Natl Health Stat Report 10(12): 1-23.

22. Trivedi MK, Patil S, Tallapragada RM (2013) Effect of biofield treatment on the physical and thermal characteristics of vanadium pentoxide powders. J Material Sci Eng S 11: 001.

23. Trivedi MK, Tallapragada RM, Branton A, Trivedi D, Nayak G, et al. (2015) Characterization of physical and structural properties of aluminum carbide powder: Impact of biofield treatment. J Aeronaut Aerospace Eng 4: 142.

24. Trivedi MK, Tallapragada RM, Branton A, Trivedi D, Nayak G, et al. (2015) The potential impact of biofield energy treatment on the atomic and physical properties of antimony tin oxide nanopowder. American Journal of Optics and Photonics 3: 123-128.

25. Trivedi MK, Branton A, Trivedi D, Nayak G, Plikerd WD, et al. (2017) A systematic study of the biofield energy healing treatment on physicochemical, thermal, structural, and behavioral properties of magnesium gluconate. International Journal of Bioorganic Chemistry 2: 135-145.

26. Trivedi MK, Branton A, Trivedi D, Nayak G, Wellborn BD, et al. (2017) Characterization of physicochemical, thermal, structural, and behavioral properties of magnesium gluconate after treatment with the Energy of Consciousness. International Journal of Pharmacy and Chemistry 3: 1-12.

27. Trivedi MK, Patil S, Shettigar H, Bairwa K, Jana S (2015) Effect of biofield treatment on spectral properties of paracetamol and piroxicam. ChemSci J 6: 98.

28. Trivedi MK, Branton A, Trivedi D, Shettigar H, Bairwa K, et al. (2015) Fourier transform infrared and ultraviolet-visible spectroscopic characterization of biofield treated salicylic acid and sparfloxacin. Nat Prod Chem Res 3: 186.

29. Trivedi MK, Branton A, Trivedi D, Nayak G, Mondal SC, et al. (2015) Effect of Biofield treated energized water on the growth and health status in chicken (*Gallus gallus domesticus*). Poult Fish WildlSci 3: 140.

30. Trivedi MK, Branton A, Trivedi D, Nayak G, Mondal SC, et al. (2015) Evaluation of biochemical marker - glutathione and DNA fingerprinting of biofield energy treated *Oryza sativa*. American Journal of BioScience 3: 243-248.

31. Trivedi MK, Branton A, Trivedi D, Nayak G, Gangwar M, et al. (2016) Molecular analysis of biofield treated eggplant and watermelon crops. Adv Crop Sci Tech 4: 208.

32. Kinney JP, Trivedi MK, Branton A, Trivedi D, Nayak G, et al. (2017) Overall skin health potential of the biofield energy healing based herbomineral formulation using various skin parameters. American Journal of Life Sciences 5: 65-74.

33. Dodon J, Trivedi MK, Branton A, Trivedi D, Nayak G, et al. (2017) The study of biofield energy treatment based herbomineral formulation in skin health and function. American Journal of BioScience 5: 42-53.

34. Trivedi MK, Branton A, Trivedi D, Nayak G, Lee AC, et al. (2017) A comprehensive analytical evaluation of the Trivedi Effect® - Energy of Consciousness Healing Treatment on the physical, structural, and thermal properties of zinc chloride. American Journal of Applied Chemistry 5: 7-18.

35. Trivedi MK, Branton A, Trivedi D, Nayak G, Plikerd WD, et al. (2017) A systematic study of the biofield energy healing treatment on physicochemical, thermal, structural, and behavioral properties of iron sulphate. International Journal of Bioorganic Chemistry 2: 135-145.

36. Brittain HG (2009) Polymorphism in pharmaceutical solids in Drugs and Pharmaceutical Sciences. (2nd edn) Informa Healthcare USA, Inc., New York.

37. Inoue M, Hirasawa I (2013) The relationship between crystal morphology and XRD peak intensity on $CaSO_4 \bullet 2H_2O$. J Cryst Growth 380: 169-175.

38. Censi R, Martino PD (2015) Polymorph impact on the bioavailability and stability of poorly soluble drugs. Molecules 20(10): 18759-18776.

39. Trivedi MK, Patil S, Tallapragada RM (2014) Atomic, Crystalline and Powder Characteristics of Treated Zirconia and Silica Powders. J Material Sci Eng 3: 144.

40. Nyquist RA, Putzig CL, Leugers MA (1997) The Handbook of Infrared and Raman Spectra of Inorganic Compounds and Organic Salts: Infrared and Raman spectral atlas of inorganic compounds and organic salts. Academic Press, Michigan.

41. Bajaj S, Singla D, Sakhuja N (2012) Stability testing of pharmaceutical products. J App Pharm Sci 2: 129-138.

42. Praserthdam P, Phungphadung J, Tanakulrungsank W (2003) Effect of crystallite size and calcination temperature on the thermal stability of single nanocrystalline chromium oxide: Expressed by novel correlation. Mater Res Innov 7: 118-123.

43. Zhao Z, Xie M, Li Y, Chen A, Li G, et al. (2015) Formation of curcumin nanoparticles *via* solution-enhanced dispersion by supercritical CO_2. Int J Nanomedicine 10: 3171-3181.

44. Moore J (2010) Chemistry: The molecular science. (4th edn) Brooks Cole.

This work is licensed under Creative Commons Attribution 4.0 License

To Submit Your Article Click Here: Submit Article

DOI: 10.32474/SJFN.2021.03.000171

SJFN

Scholarly Journal of Food And Nutrition

Scholarly Journal of Food and Nutrition

Assets of Publishing with us

- Global archiving of articles
- Immediate, unrestricted online access
- Rigorous Peer Review Process
- Authors Retain Copyrights
- Unique DOI for all articles